Biocompatible Carbon Nanotube–Chitosan Scaffold Matching the Electrical Conductivity of the Heart

Seokwon Pok,[†] Flavia Vitale,[‡] Shannon L. Eichmann,[‡] Omar M. Benavides,[†] Matteo Pasquali,[‡] and Jeffrey G. Jacot[*,†,§]

[†]Department of Bioengineering and [‡]Department of Chemical & Biomolecular Engineering, Department of Chemistry, Department of Materials Science & NanoEngineering, and The Smalley Institute for Nanoscale Science & Technology, Rice University, Houston, Texas 77005, United States and [§]Division of Congenital Heart Surgery, Texas Children's Hospital, Houston, Texas 77030, United States

ABSTRACT The major limitation of current engineered myocardial patches for the repair of heart defects is that insulating polymeric scaffold walls hinder the transfer of electrical signals between cardiomyocytes. This loss in signal transduction results in arrhythmias when the scaffolds are implanted. We report that small, subtoxic concentrations of single-walled carbon nanotubes, on the order of tens of parts per million, incorporated in a gelatin–chitosan hydrogel act as electrical nanobridges between cardiomyocytes, resulting in enhanced electrical coupling, synchronous beating, and cardiomyocyte function. These engineered tissues achieve excitation conduction velocities similar to native myocardial tissue (22 ± 9 cm/s) and could function as a full-thickness patch for several cardiovascular defect repair procedures, such as right ventricular outflow track repair for Tetralogy of Fallot, atrial and ventricular septal defect repair, and other cardiac defects, without the risk of inducing cardiac arrhythmias.

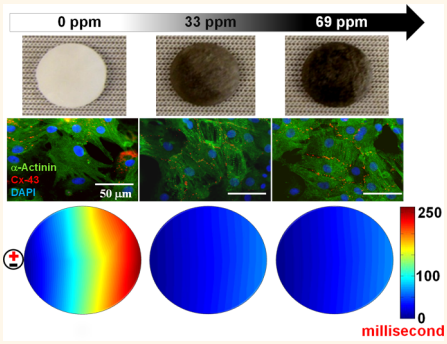

KEYWORDS: carbon nanotubes · tissue engineering · cardiomyocytes · heart defects · conduction velocity · action potential

Tetralogy of Fallot (TOF), the most common cyanotic heart defect, is a structural problem that arises from abnormal heart formation. Approximately, 5100 TOF procedures were performed in the U.S. from July 2006 to June 2010; each one generally requires surgical placement of a patch or baffle across the right ventricular outflow tract in an area that normally consists of contractile tissue.[1] An ideal cardiac patch should mimic the native extracellular matrix environment for cardiac cell support and provide the necessary framework for cell signaling molecules or growth factors.[2,3] Typical porous polymeric matrices used for cardiac tissue engineering have a number of limitations, such as pore walls that limit cell–cell interactions and delayed electrical signal propagation, which leads to an increased frequency of arrhythmias.[4,5] Structural, physiological, and mechanical properties of cardiac scaffolds have traditionally been tuned using novel and composite biomaterials,[6,7] adopting microfabrication methods,[8,9] or applying chemical cross-linking methods.[10−12] Several studies reported that the incorporation of carbon nanotubes (CNTs) in scaffolds led to improved cell adhesion, changes in cells morphogenesis and signaling, reduced material degradation rates, and altered mechanical properties.[4,13,14] These studies all incorporated relatively high concentrations of CNTs, on the order of milligrams/milliliter, which some studies suggest may be toxic to cardiomyocytes and other tissues.[15]

Single-walled carbon nanotubes (SWNTs) have the structure of a single graphite sheet rolled into a hollow tube, with diameters ranging from 0.4 to 3 nm and lengths up to tens of microns.[16] SWNTs exhibit a unique combination of mechanical strength[16,17] (Young modulus = 0.6–1.25 TPa, ~2–4 times higher than steel),[18,19] low electrical resistance (resistivity = 1 $\mu\Omega\cdot$cm, ~2 times lower than copper),[20] and high thermal

* Address correspondence to jeff.jacot@rice.edu.

Received for review July 7, 2014 and accepted September 18, 2014.

Published online September 18, 2014
10.1021/nn503693h

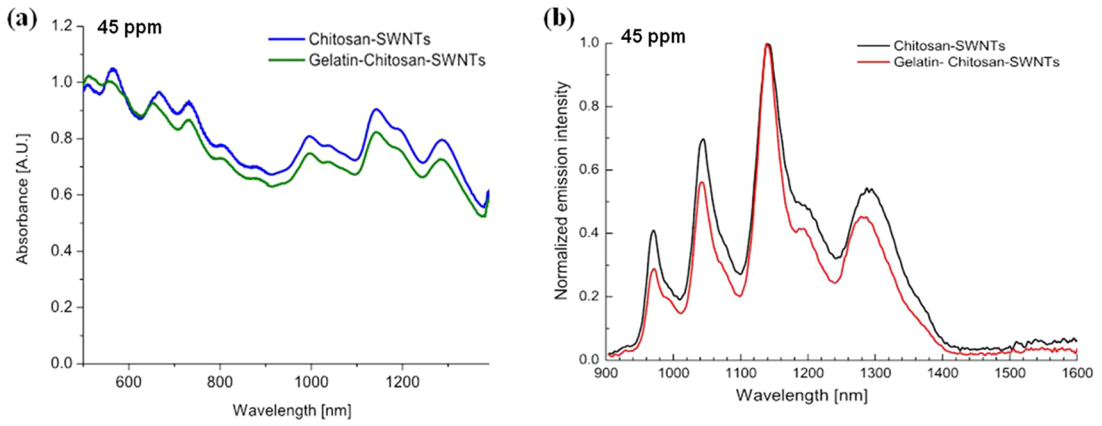

Figure 1. SWNT dispersion analysis using (a) UV−vis absorption and (b) NIR emission spectra. The SWNTs were well-dispersed at concentrations up to 350 ppm in both chitosan and gelatin−chitosan solutions.

conductivity (3000 W/m K).[21] This exceptional combination of properties makes SWNTs good candidates for a wide variety of biomedical applications such as drug[22,23] and gene delivery,[24] biosensing,[25,26] ablation of cancer cells,[27] cellular imaging,[28−30] and scaffolds for tissue engineering.[13] Irrespective of the method of synthesis or the application, the translation of the exceptional molecular properties into macroscopic assemblies still remains a challenge, mainly because of the difficulty in obtaining highly dispersed and stabilized SWNT solutions for fluid-phase processing. This difficulty originates from the strong van der Waals interactions between SWNT sidewalls. Several dispersion techniques have been adopted[31] such as covalent functionalization schemes[32,33] and protonation with superacids.[34] Functionalization generally involves the creation of defect sites on the SWNT walls, which can cause the loss of SWNTs' optical, electrical, and thermal properties.[32,35] An alternative approach consists of debundling SWNTs with sonication[36] and stabilizing with biocompatible surfactants, polymers proteins, or DNA.[37−39] Adsorption of dispersant molecules on SWNT sidewalls yields stable aqueous dispersions, without altering the SWNT properties, although the SWNTs are shortened by the sonication process.[40]

Among the different biopolymers that have been proposed as stabilizing agents for SWNTs, chitosan[41,42] is particularly viable for tissue engineering scaffolds, due to its excellent biocompatibility, biodegradability, and broad availability.[7,9,43,44] Previously, we reported on a suturable, multilayered cardiac patch made from a chitosan and gelatin composite hydrogel supported by a polycaprolactone (PCL) scaffold.[45] The PCL scaffold provides suturability and sufficient tensile strength (>2 MPa of ultimate tensile strength) for use as a cardiac patch, while the gelatin/chitosan hydrogel provides an extracellular matrix (ECM) environment for cardiac cell attachment, eventual patch degradation, and incorporation into native tissue.[46] The process of providing an electrical signal to individual cardiomyocytes early in the tissue regeneration process, however, is still a challenge.

Here we show that incorporating well-dispersed SWNTs in gelatin/chitosan solutions improves the conductivity of hydrogels even at very low concentrations (<100 ppm). Results show that the improved signal transmission from the SWNTs promotes functional maturation, improves electrical coupling, and provides synchronous beating in cardiomyocytes all while maintaining biocompatibility.

RESULTS AND DISCUSSION

Dispersion of SWNTs. SWNT bundles were dispersed in a chitosan and gelatin−chitosan solution using sonication followed by centrifugation. Figure 1 shows the UV−vis absorption and NIR emission spectra (660 nm excitation) of the SWNT dispersions in the chitosan and gelatin−chitosan mixtures after the sonication and centrifugation process. The well-resolved absorbance and emission spectra (*i.e.*, well-defined peaks) in Figure 1 indicate the presence of individually dispersed SWNTs in aqueous media;[47,48] therefore, the SWNTs were well-dispersed at concentrations up to 350 ppm in both solutions. The spectra did not change after mixing 2% chitosan−SWNTs with 2% gelatin (the mixture used for scaffold fabrication), which shows that gelatin did not affect the quality of the SWNT dispersion in aqueous chitosan solution. The absorbance and emission peaks in these solutions are not as sharp as those typically observed with the traditional surfactant solutions[47,48] but are sharper than spectra obtained with other biomolecules (*i.e.*, BSA).[38] In summary, we find that chitosan is an effective biocompatible stabilizing agent for SWNTs and that SWNTs were stable and individually dispersed in the gelatin−chitosan solutions used to prepare the scaffolds. Notably, the SWNT concentrations used here (0−175 ppm; 0−0.0175% (w/v)) are significantly lower than those in previous studies, which incorporated 0.1−1.3% CNTs to achieve electrical conduction through the hydrogel[49,50]

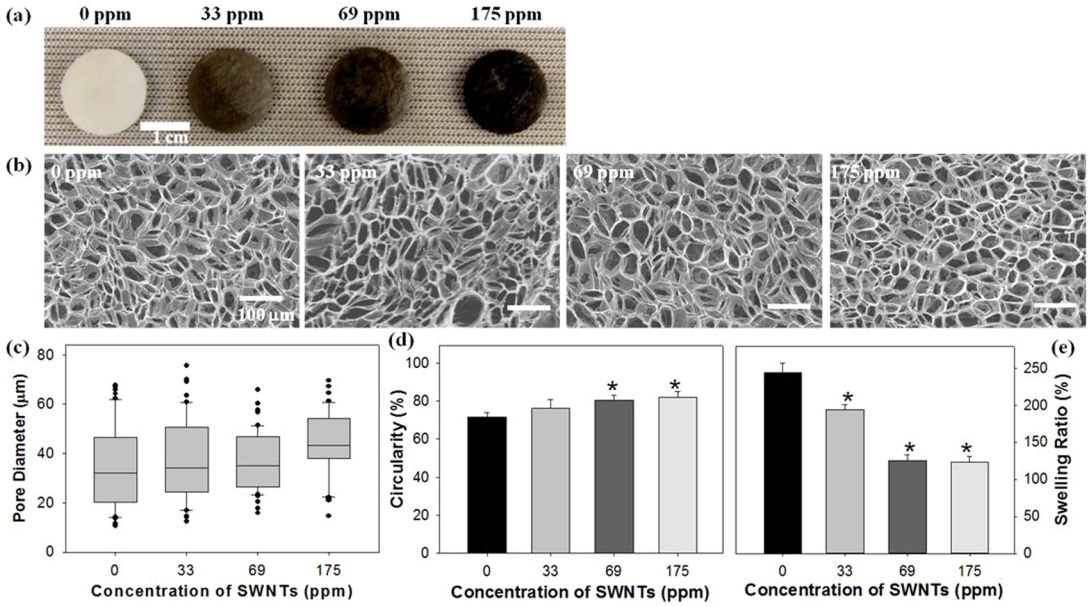

Figure 2. Macro- and microscopic structural properties of SWNT-incorporated hydrogels: (a) macrograph and (b) SEM micrographs of SWNT hydrogels with different concentrations. Effects of the concentration of SWNTs on (c) pore diameter, (d) circularity, and (e) swelling ratio of hydrogels; *$p < 0.05$, $n = 5$.

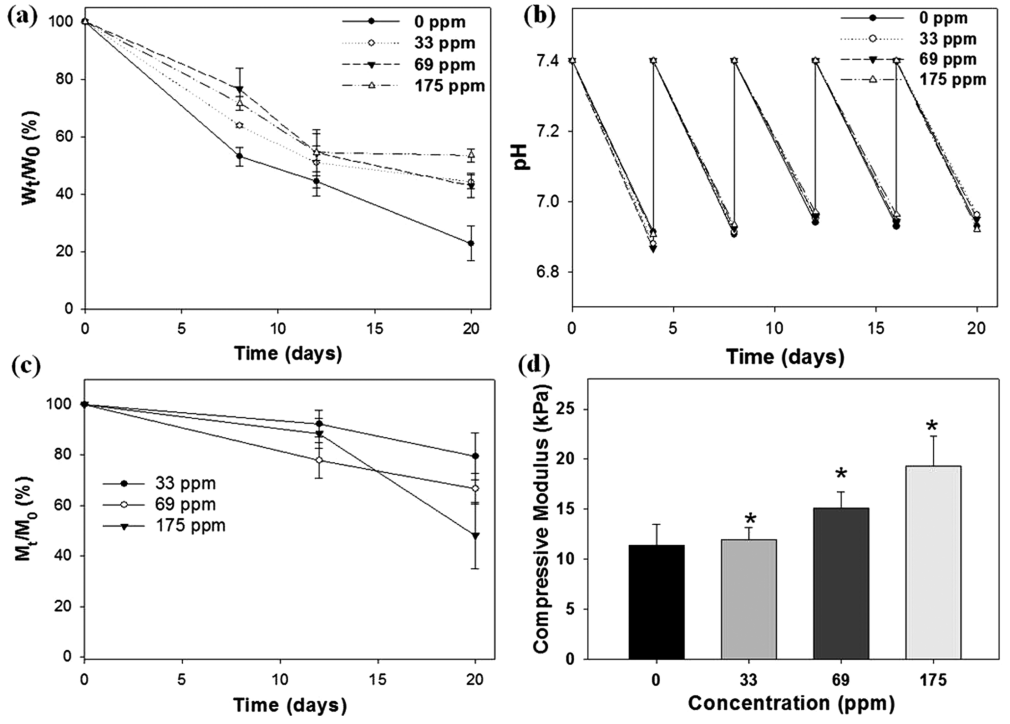

Figure 3. Effects of SWNT concentration on *in vitro* degradation and compressive modulus: (a) weight loss of scaffolds, (b) pH changes, (c) mass loss of SWNTs during degradation, and (d) compressive modulus. Hydrogels with SWNTs showed significantly slower degradation and increased compressive modulus; *$p < 0.05$, $n = 5$.

(likely due to CNT bundling and lower dispersion quality of the CNTs throughout the hydrogel matrix).

Physical Characteristics of Hydrogels Containing SWNTs. Scaffold porosity, pore interconnectivity, and suitable flow channels need to be present for adequate cell invasion, transport of nutrients and waste, and transduction of cellular signals. The circularity is also a desirable factor as a cell delivery system because circular pores having a larger area than cells can promote the pathway for cell invasion. Further, since our gelatin–chitosan scaffold is geometrically anisotropic, the circular structure can distribute uniform mechanical stresses through the scaffold. Each of these properties is a prerequisite of proper tissue regeneration in hydrogels.[51] Previous studies have demonstrated that incorporating CNTs alters the morphological

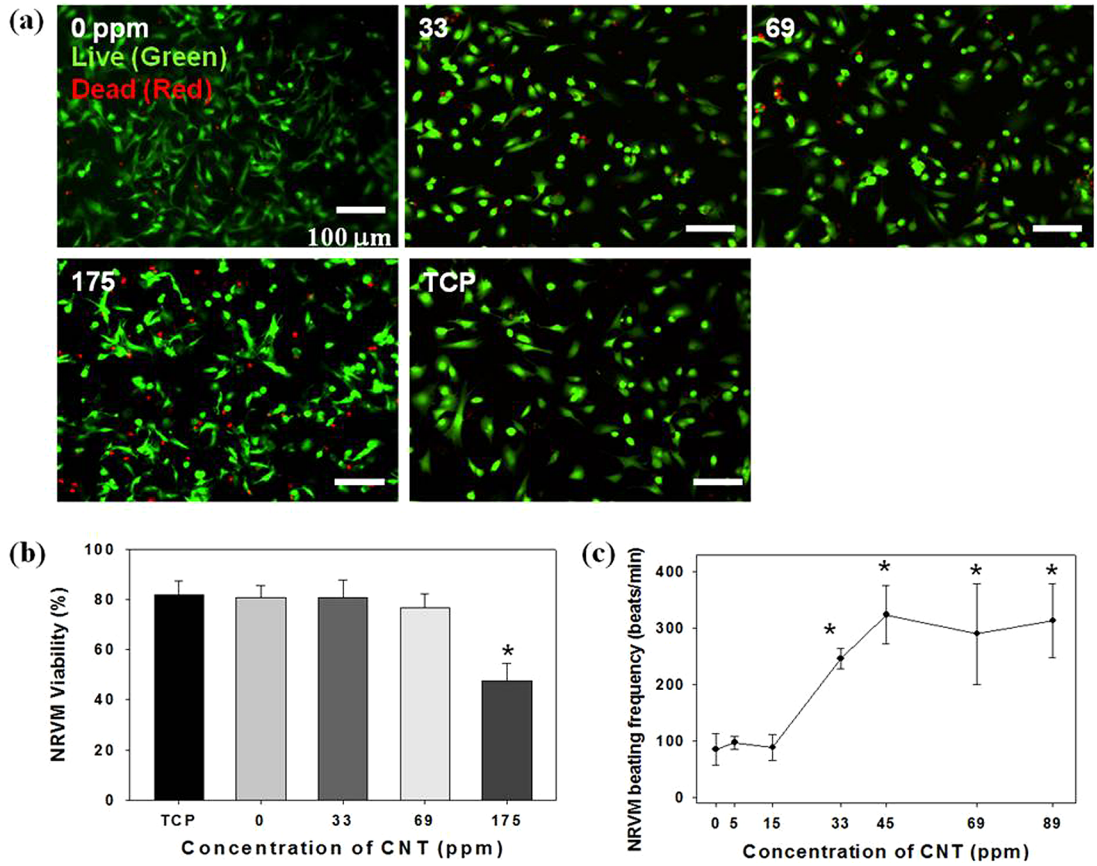

Figure 4. Effects of SWNT concentration on (a,b) ventricular myocyte viability and (c) spontaneous beating frequency. At 175 ppm, samples showed significantly decreased myocyte viability after 4 days in culture (47 ± 7%; $p < 0.05$, $n = 5$). Myocytes grown on 69 ppm or higher concentrations of SWNTs had a consistent rate of ~310 beats/min, approaching the beating frequency of rat hearts ($p < 0.05$, $n = 10$).

properties of hydrogels or tissues due to the formation of supramolecular hybrid hydrogels with a strong CNT backbone.[52,53] Figure 2 shows the effects of SWNT incorporation on morphological and structural properties. Hydrogels containing SWNTs showed the same sponge-like matrix after lyophilization as those without SWNTs; higher SWNT concentration yielded darker samples (Figure 2a). Additionally, SEM analysis showed that all samples had similar anisotropic and symmetric porous structures (Figure 2b) irrespective of SWNT concentration. There was no significant effect of SWNT concentration on the mean pore diameter; however, hydrogels with SWNT concentrations of 69 ppm and higher had more uniform pore diameter distributions than those hydrogels with lower SWNT concentrations (Figure 2c). Finally, the circularity of the pores increased significantly with increasing SWNT concentration (circularity (%); 71.6 ± 2.3 in 0 ppm, 80.2 ± 2.8 in 69 ppm, 81.8 ± 3.4 in 175 ppm; $p < 0.05$, $n = 5$) (Figure 2d). This might be due to the changes in cohesion of the solutions during freeze-drying.[54] Previous studies also demonstrated that the viscosity of solution was increased by dispersion of SWNTs[55] Higher viscosity resulted in slower ice crystal formation that allows neighboring crystals to exert a compressive force on each other and can compact themselves into a more circular arrangement.[54]

One common feature of engineered hydrogels made from natural components is a high swelling ratio that drastically weakens the mechanical strength during tissue regeneration.[56] The swelling ratio of the hydrogels was evaluated after 48 h of incubation in cell culture media at 37 °C. The 69 and 175 ppm of SWNT hydrogels had a significantly lower swelling ratio than the baseline chitosan gel (no SWNTs) and 33 ppm of SWNT hydrogels (swelling ratio (%); 244 ± 13 in 0 ppm, 193 ± 7 in 33 ppm, 124 ± 8 in 69 ppm, 123 ± 8 in 175 ppm; $p < 0.05$, $n = 5$) (Figure 2d).

The effect of SWNT concentration on the degradation rate and compressive modulus of the hydrogels was evaluated in physiological conditions. All samples had ~40% weight loss after 2 weeks of incubation with no significant difference observed between samples over time ($p > 0.05$, $n = 5$) (Figure 3a). Samples without SWNTs showed a linear decrease ($R^2 = 91\%$) in weight and lost ~80% of their weight after 3 weeks of incubation. Samples containing SWNTs, however, showed significantly slower degradation during the period of 2−3 weeks, likely as a result of increased hydrophobicity. A similar reduction in pH was observed every

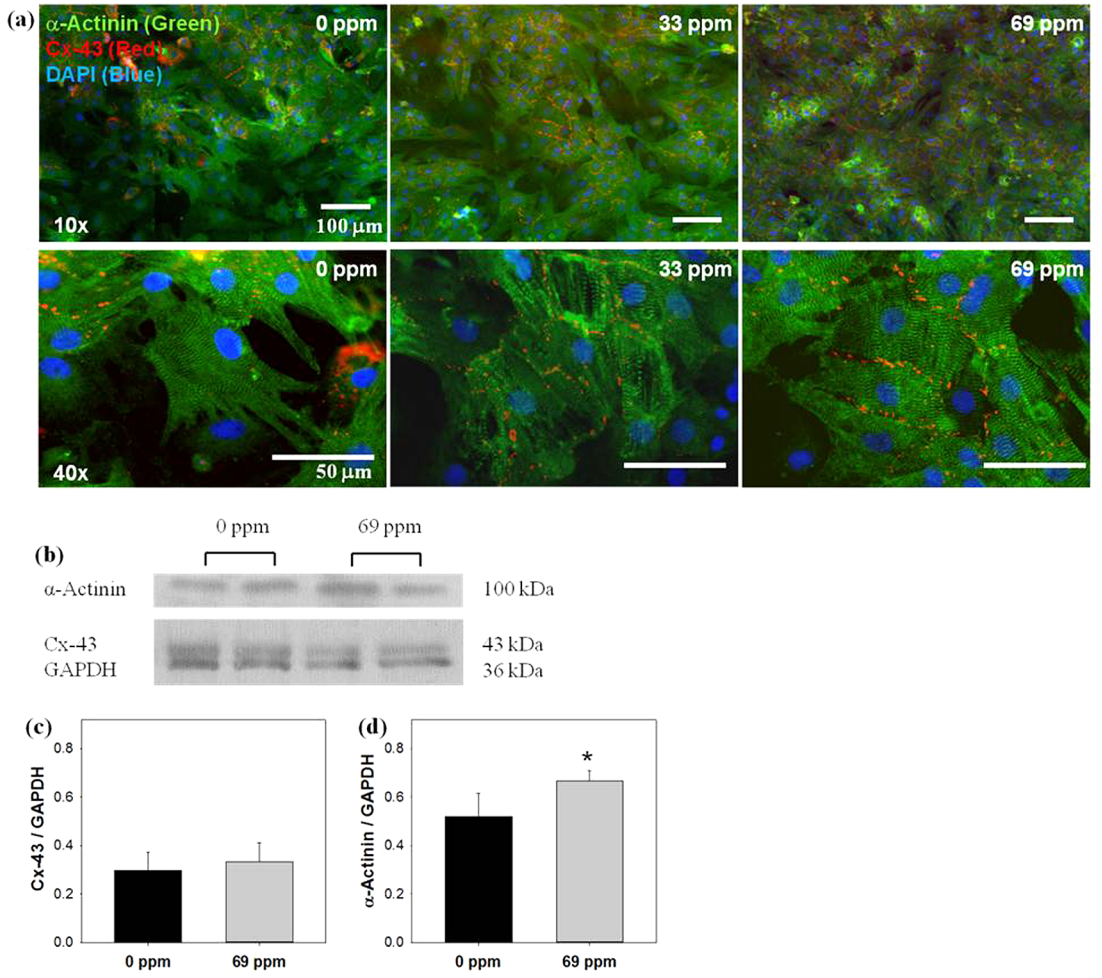

Figure 5. Ventricular myocytes cultured on hydrogels stained for (a) sarcomeres (α-actinin = green), gap junctions (connexin-43 = red), and DNA (DAPI). (b) Quantification of protein expression using Western blot analysis for (c) connexin-43 and (d) α-actinin. The sarcomeres and gap junctions are clearly visible and quantified, suggesting that the upregulation of α-actinin leads to improved cardiomyocyte contractile function; *$p < 0.05$, $n = 5$.

4 days in all samples (Figure 3b). Moreover, after 20 days of degradation, a significantly larger percentage (~50%) of SWNTs was released from samples loaded with 175 ppm (Figure 3c) compared to samples loaded with lower concentrations of SWNTs. Samples loaded with 33 and 69 ppm of SWNTs released ~21 and 33% of the loaded SWNTs after 20 days of degradation, respectively (Figure 3c). Previous studies demonstrated that CNT-based materials have significantly higher mechanical strength due to the CNT sp^2 carbon–carbon bonds.[57,58] Our results also indicated that hydrogels with SWNTs had a 65% increase in compressive modulus when SWNT concentration was increased from 0 to 175 ppm. Hydrogels with SWNT concentrations of 69 ppm or higher had much higher compressive moduli than hydrogels containing 0 or 33 ppm of SWNTs (11.4 ± 2.0 kPa of 0 ppm, 15.1 ± 1.2 kPa of 69 ppm, 19.3 ± 3.0 kPa of 175 ppm; $p < 0.05$; $n = 5$) (Figure 3d). There was no significant difference in compressive modulus between hydrogels containing 0 and 33 ppm of SWNTs. A previous study also reported that the incorporation of CNTs in polypropylene biocomposites increased the stiffness of hydrogels by 67% when increasing CNT concentration from 0 to 0.3% w/v (=3000 ppm).[49]

Ventricular Myocyte Viability and Beating Frequency. The literature is divided on the cytotoxicity of carbon nanotubes. Here we studied the effect of SWNT concentration on cell viability to establish the optimal conditions for cardiomyocytes cultured in gelatin–chitosan hydrogels by live–dead cell immunostaining after 4 days in culture (Figure 4a). Neonatal rat ventricular myocytes (NRVM) cultured in hydrogels with SWNT concentrations of 69 ppm or lower had >80% viability and showed no significant difference in cell viability compared to NRVM cultured on control tissue culture plastic. However, at 175 ppm, samples showed significantly reduced NRVM viability (47.7 ± 6.9%; $p < 0.05$, $n = 5$) (Figure 4b), suggesting that potential SWNT toxicity may be dose-dependent. A recent study by Mooney *et al.* also showed that concentrations of CNT above 0.032 mg/mL (=32 ppm) adversely affected the viability of mesenchymal stem-cell-derived cardiomyocytes.[59]

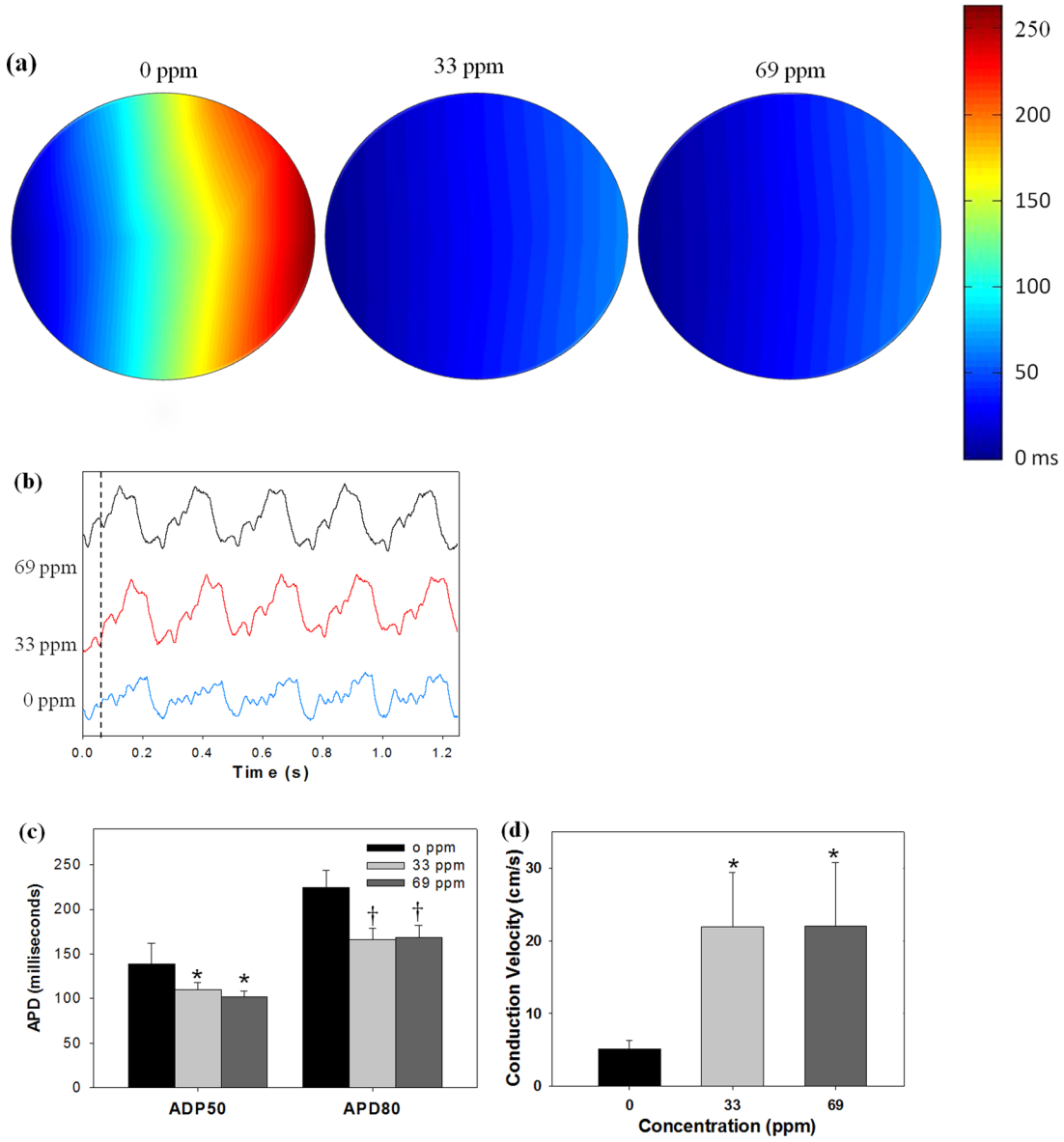

Figure 6. Ventricular myocyte stained with Di-8-ANEPPS after 7 days in culture. (a) Optical maps of activation time, (b) action potential signal, (c) action potential duration (APD) at 50 and 80% of return to baseline amplitude, and (d) conduction velocity. Hydrogels containing SWNTs showed significantly reduced APD (both 50 and 80%; $p < 0.05$, $n = 5$) and significantly faster conduction velocity ($p < 0.05$, $n = 5$) compared to pure engineered tissues.

The SWNT concentration also affected the spontaneous beating frequency of NRVM. NRVM in all samples started beating regionally after 3−4 days in culture and synchronously after 6−8 days in culture. Samples below 33 ppm showed a similar beating frequency as the samples without SWNTs (~100 beats/min) (Figure 4c), well below the natural beating frequency of rat hearts (330−480 beats/min). The beating rate of the cells increased significantly on scaffolds with SWNT concentrations higher than 33 ppm ($p < 0.05$, $n = 10$). The beating rate of 33 ppm of SWNT samples was ~240 beats/min, and NRVM grown on 69 ppm or higher concentrations of SWNTs had a consistent rate of ~310 beats/min, approaching the beating frequency of rat hearts (Figure 4c).

Ventricular Myocyte Functionalization and Action Potential. The cell morphology of NRVM was evaluated by immunostaining after 7 days of culture (Figure 5). After 7 days, all samples had well spread myocytes (Figure 5a) in close contact and all hydrogels showed spontaneous beating. Figure 5a also indicates that ventricular myocytes on all samples showed clearly expressed sarcomeres (α-actinin = green) and gap junctions (connexin-43 = red) demonstrating interconnected and integrated myocytes. However, these cells had a different cell morphology compared to cells in viability studies. This is probably due to the greater number of fibroblasts resulting from the higher initial cell density and longer culturing time (4 days *vs* 7 days). In addition, the shape of the cardiomyocytes is different than

typical aligned cardiomyocytes because cells spread anisotropically through the anisotropic porous structure of the scaffold. Western blot analysis for protein expression revealed that the inclusion of SWNTs in gelatin–chitosan hydrogels significantly increased α-actinin expressions ($p < 0.05$, $n = 5$) while minimally affecting connexin-43 expression (Figure 5b–d). In Figure 5a, the sarcomeres and gap junctions are clearly visible. This suggests that the upregulation of α-actinin in NRVMs plated on hydrogels containing SWNTs leads to more mature cardiomyocyte contractile function. This is supported by both the increase in NRVM beating frequency and the increase in NRVM conduction velocity. Though an increase in connexin-43 was not seen between samples, hydrogels containing SWNTs clearly expressed a more physiologically relevant localization of connexin-43 to localized gap junction formations at cell–cell junctions than hydrogels without SWNTs. As a result, the increased number of functional gap junctions between NRVMs could also play a role in increasing beating frequency and conduction velocity.[60]

In vitro assessment of action potential properties was performed in NRVM in gelatin–chitosan composite hydrogels with and without SWNTs after 7 days in culture, using a voltage-sensitive dye (Di-8-ANEPPS). Conduction velocity of the action potential depends on two main factors: intercellular electrical coupling and cellular electrical excitability.[60] Figure 6a shows the activation time propagation, and Figure 6b presents an action potential signal from NRVM cultured on hydrogels. Our results show that the propagation of conduction velocity was strongly affected by the presence of SWNTs (Figure 6a). The conduction velocity of NRVM cultured in hydrogels containing SWNTs was ~23 cm/s, which is significantly faster than NRVM cultured in hydrogels without SWNTs. This was also faster than what was previously reported in engineered cardiac tissues and similar to that of native neonatal cardiac tissues: previous literature reports ~15 cm/s when NRVM are cultured on poly(glycolic acid),[5] ~14 cm/s when cultured on collagen sponge,[61] 8 cm/s when cultured on gelatin–chitosan, and ~27 cm/s in 10 day old neonatal rat heart.[62] Furthermore, SWNT incorporation also caused a decrease of action potential duration (APD) at both 50% (APD_{50}) and 80% (APD_{80}) of repolarization and had similar APD to native neonatal cardiomyocytes (~120 ms of APD_{80}).[63] Both APD_{50} and APD_{80} of engineered tissues containing SWNTs were significantly reduced compared to pure engineered tissues (APD_{50} of 139 ± 23 ms at 0 ppm, 110 ± 8 ms at 33 ppm, 102 ± 6 ms at 69 ppm; APD_{80} of 224 ± 20 ms at 0 ppm, 166 ± 13 ms at 33 ppm, 169 ± 14 ms at 69 ppm; $p < 0.05$, $n = 5$) (Figure 6c). Quantitatively, the results show that the average conduction velocity (CV) of NRVM cultured on hydrogels containing SWNTs was significantly faster than on pure hydrogels (CV of 5.2 ± 1.2 cm/s in 0 ppm, 21.9 ± 7.4 cm/s in 33 ppm, 22.0 ± 8.7 cm/s in 69 ppm; $p < 0.05$, $n = 5$) (Figure 6d). These results confirm that SWNTs enhanced cellular electrical excitability and lead to more mature action potential properties in cardiomyocytes.

CONCLUSIONS

These results demonstrate that introducing small amounts of well-dispersed, high-quality SWNTs into a chitosan-based hydrogel supports cardiomyocyte functionalization and greatly speeds up conduction velocity, nearly attaining the natural beating rate of rat hearts. Tissue engineered scaffolds with these properties would make improved myocardial patches for a full-thickness defect patch in right ventricular outflow track repair for Tetralogy of Fallot, repair of septal defects, and other heart defects. Future research will involve testing SWNTs' gelatin–chitosan scaffold *in vivo* in a full-thickness defect right ventricle patch in a rat model.

METHODS

Dispersion of Carbon Nanotubes. Single-walled carbon nanotubes were purchased from Carbon Nanotechnologies (HiPco batch 195.3). The SWNTs were used as-received, without further purification or functionalization procedures. HiPco SWNTs are typically composed of 60% semiconducting and 40% metallic tube species;[64] the sample purity is >90%,[65–67] and the size distribution ranges from 0.7 to 1.3 nm, with an average diameter of 0.98 ± 0.21 nm.[47,65,68] SWNTs show a wide length polydispersity, with length distribution ranging from 0.1 to 4 μm;[65,69,70] however, the sonication process used to disperse SWNTs in aqueous solutions shortens the tubes to an average length that depends on the sonication time and power.[71] The average length of SWNTs used in this work after sonication in the 2% chitosan solution was 262 ± 6 nm, obtained from shear rheology measurements[70,72] assuming a chitosan diameter of 0.845 nm.[73] SWNTs were incorporated into gelatin/chitosan composite hydrogels using previously described procedures with slight modifications.[45,74] Briefly, 500 ppm (0.5 mg/mL) SWNTs were dispersed in 0.5 M acetic acid chitosan (2% w/v, Sigma-Aldrich, St. Louis, MO) solution using a tip-sonicator (model S-4000-010, Misonix, NY) at 12 W for 15 min. After sonication, the solution was centrifuged for 2 h at 13 000 rpm to remove undispersed SWNT aggregates. The supernatant was then collected and recentrifuged for an additional 1 h at 13 000 rpm to further separate debundled tubes from remaining aggregates. UV–vis–NIR absorption and SWNT photoluminescence spectra were collected with NS1 NanoSpectralyzer (Applied NanoFluorescence, TX) to characterize the quality of the SWNT dispersions using a 2% chitosan solution as reference. SWNT fluorescence was excited at 660 nm, and emission was detected between 900 and 1400 nm. SWNT–chitosan solutions were then diluted with 2% chitosan solution to attain the desired concentration and then mixed with gelatin solution (2% w/v, type A, Sigma-Aldrich, St. Louis, MO). Next, 250 μL of the SWNT–chitosan–gelatin solution was poured into a custom Teflon mold to produce a disk, followed by lyophilization at −50 °C for 24 h. Formed scaffolds were neutralized using 100% ethanol and rehydrated using phosphate buffered saline (PBS).

Measurement of SWNT Concentration and Porosity. Lyophilized samples were allowed to dry overnight in a vacuum desiccator at room temperature. The diameter and thickness of dry matrices were measured to calculate the volume, and then samples were attached to aluminum stubs with carbon tape and sputter-coated with gold for 1 min. Surface architecture of the scaffolds was analyzed using a scanning electron microscope (JEOL 6360, Jeol USA Inc., Peabody, MA) at an accelerating voltage of 15 kV. Images were analyzed for the average pore diameter and circularity (n = 15 on 4 different samples) using ImageJ. Swelling ratio was also evaluated by calculating the ratio of the volumes of wet samples to the volume of dry samples. The volume of wet samples was measured after 48 h incubation in PBS at 37 °C.

Measurement of Degradation Rate and Compressive Modulus. Degradation rates of samples were analyzed using a previously described procedure with minor modifications.[45] Briefly, 6 mm diameter samples were cut from samples containing different SWNT concentrations, washed with deionized water, sterilized in 70% ethanol for 1 h, and washed thoroughly in sterile Krebs–Henseleit buffer solution (119 mM NaCl, 4.7 mM KCl, 25 mM $NaHCO_3$, 2.5 mM $CaCl_2$, 1.2 mM KH_2PO_4, 1.2 mM $MgSO_4$) prior to incubation in 10 mL of Krebs–Henseleit buffer solution (pH 7.4). Samples were placed in 12-well plates, and incubation was carried out in an incubator maintained at 37 °C and 5% CO_2/95% air. The weight of samples was measured every 4 days. During incubation, the pH of the effluent was measured and maintained at 7.4 by replacing the buffer solution once every 4 days. The amount of SWNT in the scaffolds after 12 and 20 days of the degradation process was determined using a published procedure with minor modifications.[34,75−77] Scaffolds were lyophilized for 12 h at −55 °C. Then samples were weighed, mixed with 2 mL of chlorosulfonic acid, and magnetically stirred for 3 h to allow for complete dissolution of the scaffolds. UV–vis–NIR absorption spectra in the range of 550 to 1100 nm were collected on a Shimadzu UV-1800 spectrophotometer using 1 cm path length quartz cuvettes covered with Teflon caps. The value of absorbance at 1000 nm, where absorbance from both gelatin and chitosan becomes negligible,[78−80] was used to calculate SWNT concentration in the solution of chlorosulfonic acid by comparison to a calibration curve of absorbance *versus* SWNT concentration.

The compressive modulus of hydrogels was also measured to find the effect of different SWNT concentration (0, 33, 69, and 175 ppm) using a previously described procedure with minor modifications.[45] Samples were neutralized using 100% ethanol and rehydrated using PBS, then hydrogels were preconditioned in high-serum plating media (Dulbecco's modified Eagle medium, 17% M199, 10% horse serum, 5% fetal bovine serum, 100 U/mL penicillin, and 50 mg/mL streptomycin) at 37 °C for 24 h. Hydrogels (n = 5) were placed in stainless steel platens in an Instron 5942 (Norwood, MA) and compressed up to 3% strain (~100 μm) at 10 μm/s of load speed. The load–displacement data were then converted into compression stress.

Neonatal Rat Ventricular Myocyte Isolation and Culture. All studies involving experimental animals were approved by the Institutional Animal Care and Use Committees of both Rice University and Baylor College of Medicine. Neonatal rat ventricular myocytes were isolated from 1–3 day old Sprague–Dawley rat hearts as described previously.[81] Briefly, rats were anesthetized with isoflurane, decapitated, and the hearts removed. Blood vessels and atria were trimmed, leaving only the ventricles. Ventricular cardiomyocytes were isolated using enzymatic digestion with an isolation kit (Cellutron, Highland Park, NJ). Isolated cells were preplated in Petri dishes for 2 h to remove fibroblasts and endothelial cells. Unattached cells at 0.5–3 × 10^6 cells in 2 mL of high-serum plating media were seeded onto each hydrogel. After 24 h, cell seeded samples were transferred to a low serum media (Dulbecco's modified Eagle medium, 18.5% M199, 5% horse serum, 1% fetal bovine serum, and antibiotics). Cell cultures were maintained at 37 °C and 5% CO_2/95% air, and fresh maintenance medium was added every day. All culture medium was purchased from Invitrogen (Carlsbad, CA), and serum was purchased from PAA Laboratories (Ontario, Canada).

Immunofluorescence Analysis. Cardiomyocyte adhesion, morphology, and viability on hydrogels were analyzed. For viability testing, 0.5 × 10^6 cells were seeded onto hydrogels and cultured for 4 days. For cell adhesion and morphology testing, 3.0 × 10^6 cells were seeded onto hydrogels and cultured for 7 days. All samples were maintained in 5% CO_2/95% air at 37 °C with medium changed every 24 h. Cells were then washed in cold (4 °C) PBS and fixed in 4% paraformaldehyde (Electron Microscopy Sciences) for 20 min at 4 °C. Cells were washed with PBS and made permeable with 0.5% Triton X100 (Sigma). Cells were again washed in PBS and stained with Alexa Fluor 488 Phalloidin (Invitrogen Corp., Eugene, OR) at a 1:1000 dilution in 1% bovine serum albumin (BSA, Gemini Bioproducts) overnight at 4 °C. Cells were then counterstained with DAPI-containing Vecta Shield (Vector, Burlingame, CA). Images were obtained using a DMI 6000B (Leica Microsystems, Bannockburn, IL) fluorescence microscope to analyze cell adhesion and morphology. Primary and secondary antibodies of cardiac cell markers were also used to characterize NRVM morphologies. Monoclonal anti-α-actinin (1:400, Sigma-Aldrich, MO) and anti-connexin-43/GJA1 (1:400, Abcam, MA) were used to visualize sarcomeres and gap junctions, respectively. Antibodies were used at a 1:400 dilution in 1% BSA and incubated for 1 h at room temperature. Secondary antibodies of DyLight 488-conjugated goat anti-mouse (1:400, JacksonIR, PA) and 549-conjugated goat anti-rabbit were used at 1:400 dilutions in 1% BSA and incubated for 30 min at room temperature followed by four 1% BSA washes. Additionally, NRVM were cultured on multilayered scaffolds for 4 days and stained with live/dead assay reagents (Invitrogen Corp., Eugene, OR) to determine cell viability.

Measurement of Conduction Velocity. Conduction velocity of NRVM on gelatin or heart matrix scaffolds was analyzed using the voltage sensitive dye Di-8 ANEPPS (Enzo Life Science, Farmingdale, NY) and an IonOptix system (IonOptix LLC, Milton, MA) followed by manufacturer's and previously described procedures with modifications.[82,83] Briefly, spontaneously beating scaffolds with 7 day cultured NRVM were transferred to a 35 mm Petri dish and covered with 2 mL of warm Tyrode's solution (pH = 7.4) of the following composition: 130 NaCl, 5.4 KCl, 1 $MgCl_2$, 0.3 Na_2HPO_4, 5.5 D-glucose, 10 HEPES, 2 $CaCl_2$ in mmol/L. Then, 2 mL of Di-8 ANEPPS (2 mM) in DMSO was added to the Petri dish and, scaffolds were incubated for 13 min after being covered with aluminum foil. Stained scaffolds were transferred to a custom-built chamber that maintained the temperature of the Tyrode's solution at 37 °C. Cells were stimulated though platinum electrodes on the side of the scaffold with the following settings: 0.5–1 Hz, 5 V, 10 ms duration, and bipolar. Action potential signals at 11 different positions were measured while electrodes were fixed in the same position throughout the experiment. Conduction velocity was calculated by measuring the activation time to 50% of action potential magnitude as well as the distance between electrodes and the positions where signals were obtained. Action potential duration (APD_{50} and APD_{80}) was determined by measuring the repolarization time to 50 and 80% of return to baseline amplitude.

Statistical Analysis. Cell culture experiments were repeated three to six times with quadruplicate samples. Mechanical testing was repeated four or more times. Specific repeat numbers are noted in figure captions. Results are reported as mean ± standard deviation. Significant differences between two groups were evaluated using analysis of variance with 95 or 99% confidence intervals, then paired differences were tested with a post-hoc t test with a Bonferroni–Dunn correction for multiple comparisons. When $p < 0.05$, the differences were considered to be statistically significant.

Conflict of Interest: The authors declare no competing financial interest.

Acknowledgment. We would like to thank Dr. Mikos in the Department of Bioengineering at Rice University for the use of the lyophilizer, Dr. Theresa Hsu for the help with rheology measurements, and Robert Headrick for the support with the scaffold degradation studies. This work was supported by the NIH R21NL110330 (to J.G.J.), Welch Foundation C-1668, and Texas Children's Hospital.

REFERENCES AND NOTES

1. Go, A. S.; Mozaffarian, D.; Roger, V. L.; Benjamin, E. J.; Berry, J. D.; Blaha, M. J.; Dai, S.; Ford, E. S.; Fox, C. S.; Franco, S.; *et al.* Heart Disease and Stroke Statistics—2014 Update: A Report From the American Heart Association. *Circulation* **2014**, *129*, e28–e292.
2. Martins-Junior, P. A.; Alcantara, C. E.; Resende, R. R.; Ferreira, A. J. Carbon Nanotubes: Directions and Perspectives in Oral Regenerative Medicine. *J. Dent. Res.* **2013**, *92*, 575–583.
3. Bottino, M. C.; Thomas, V.; Schmidt, G.; Vohra, Y. K.; Chu, T.-M. G.; Kowolik, M. J.; Janowski, G. M. Recent Advances in the Development of GTR/GBR Membranes for Periodontal Regeneration—A Materials Perspective. *Dent. Mater.* **2012**, *28*, 703–721.
4. Dvir, T.; Timko, B. P.; Brigham, M. D.; Naik, S. R.; Karajanagi, S. S.; Levy, O.; Jin, H.; Parker, K. K.; Langer, R.; Kohane, D. S. Nanowired Three-Dimensional Cardiac Patches. *Nat. Nanotechnol.* **2011**, *6*, 720–725.
5. Bursac, N.; Loo, Y.; Leong, K.; Tung, L. Novel Anisotropic Engineered Cardiac Tissues: Studies of Electrical Propagation. *Biochem. Biophys. Res. Commun.* **2007**, *361*, 847–853.
6. Radhakrishnan, J.; Krishnan, U. M.; Sethuraman, S. Hydrogel Based Injectable Scaffolds for Cardiac Tissue Regeneration. *Biotechnol. Adv.* **2014**, *32*, 449–461.
7. Pok, S.; Benavides, O. M.; Hallal, P.; Jacot, J. G. Use of Myocardial Matrix in a Chitosan-Based Full-Thickness Heart Patch. *Tissue Eng., Part A* **2014**, *20*, 1877–1887.
8. Weining, B.; Christopher, P. J.; Nenad, B. Controlling the Structural and Functional Anisotropy of Engineered Cardiac Tissues. *Biofabrication* **2014**, *6*, 024109.
9. Ma, X.; Ge, J.; Li, Y.; Guo, B.; Ma, P. X. Nanofibrous Electroactive Scaffolds from Chitosan-Grafted-Aniline Tetramer by Electrospinning for Tissue Engineering. *RSC Adv.* **2014**, *4*, 13652–13661.
10. Wieland, J. A.; Houchin-Ray, T. L.; Shea, L. D. Non-viral Vector Delivery from PEG-Hyaluronic Acid Hydrogels. *J. Controlled Release* **2007**, *120*, 233–241.
11. Balakrishnan, B.; Jayakrishnan, A. Self-Cross-Linking Biopolymers as Injectable *In Situ* Forming Biodegradable Scaffolds. *Biomaterials* **2005**, *26*, 3941–3951.
12. Moffat, K. L.; Marra, K. G. Biodegradable Poly(ethylene glycol) Hydrogels Crosslinked with Genipin for Tissue Engineering Applications. *J. Biomed. Mater. Res., Part B* **2004**, *71*, 181–187.
13. Cha, C.; Shin, S. R.; Annabi, N.; Dokmeci, M. R.; Khademhosseini, A. Carbon-Based Nanomaterials: Multifunctional Materials for Biomedical Engineering. *ACS Nano* **2013**, *7*, 2891–2897.
14. Correa-Duarte, M. A.; Wagner, N.; Rojas-Chapana, J.; Morsczeck, C.; Thie, M.; Giersig, M. Fabrication and Biocompatibility of Carbon Nanotube-Based 3D Networks as Scaffolds for Cell Seeding and Growth. *Nano Lett.* **2004**, *4*, 2233–2236.
15. Garibaldi, S.; Brunelli, C.; Bavastrello, V.; Ghigliotti, G.; Nicolini, C. Carbon Nanotube Biocompatibility with Cardiac Muscle Cells. *Nanotechnology* **2006**, *17*, 391–397.
16. Baughman, R. H.; Zakhidov, A. A.; de Heer, W. A. Carbon Nanotubes—The Route toward Applications. *Science* **2002**, *297*, 787–792.
17. De Volder, M. F. L.; Tawfick, S. H.; Baughman, R. H.; Hart, A. J. Carbon Nanotubes: Present and Future Commercial Applications. *Science* **2013**, *339*, 535–539.
18. Salvetat, J.-P.; Briggs, G. A. D.; Bonard, J.-M.; Bacsa, R. R.; Kulik, A. J.; Stöckli, T.; Burnham, N. A.; Forró, L. Elastic and Shear Moduli of Single-Walled Carbon Nanotube Ropes. *Phys. Rev. Lett.* **1999**, *82*, 944–947.
19. Lu, J. Elastic Properties of Carbon Nanotubes and Nanoropes. *Phys. Rev. Lett.* **1997**, *79*, 1297–1300.
20. Tans, S. J.; Devoret, M. H.; Dai, H.; Thess, A.; Smalley, R. E.; Geerligs, L. J.; Dekker, C. Individual Single-Wall Carbon Nanotubes as Quantum Wires. *Nature* **1997**, *386*, 474–477.
21. Hone, J.; Whitney, M.; Piskoti, C.; Zettl, A. Thermal Conductivity of Single-Walled Carbon Nanotubes. *Phys. Rev. B* **1999**, *59*, R2514–R2516.
22. Bhirde, A. A.; Patel, V.; Gavard, J.; Zhang, G.; Sousa, A. A.; Masedunskas, A.; Leapman, R. D.; Weigert, R.; Gutkind, J. S.; Rusling, J. F. Targeted Killing of Cancer Cells *in Vivo* and *in Vitro* with EGF-Directed Carbon Nanotube-Based Drug Delivery. *ACS Nano* **2009**, *3*, 307–316.
23. Lacerda, L.; Raffa, S.; Prato, M.; Bianco, A.; Kostarelos, K. Cell-Penetrating CNTs for Delivery of Therapeutics. *Nano Today* **2007**, *2*, 38–43.
24. Herrero, M. A.; Toma, F. M.; Al-Jamal, K. T.; Kostarelos, K.; Bianco, A.; Da Ros, T.; Bano, F.; Casalis, L.; Scoles, G.; Prato, M. Synthesis and Characterization of a Carbon Nanotube—Dendron Series for Efficient siRNA Delivery. *J. Am. Chem. Soc.* **2009**, *131*, 9843–9848.
25. Cella, L. N.; Chen, W.; Myung, N. V.; Mulchandani, A. Single-Walled Carbon Nanotube-Based Chemiresistive Affinity Biosensors for Small Molecules: Ultrasensitive Glucose Detection. *J. Am. Chem. Soc.* **2010**, *132*, 5024–5026.
26. Heller, D. A.; Jin, H.; Martinez, B. M.; Patel, D.; Miller, B. M.; Yeung, T.-K.; Jena, P. V.; Höbartner, C.; Ha, T.; Silverman, S. K.; *et al.* Multimodal Optical Sensing and Analyte Specificity Using Single-Walled Carbon Nanotubes. *Nat. Nanotechnol.* **2009**, *4*, 114–120.
27. Gannon, C. J.; Cherukuri, P.; Yakobson, B. I.; Cognet, L.; Kanzius, J. S.; Kittrell, C.; Weisman, R. B.; Pasquali, M.; Schmidt, H. K.; Smalley, R. E.; *et al.* Carbon Nanotube-Enhanced Thermal Destruction of Cancer Cells in a Noninvasive Radiofrequency Field. *Cancer* **2007**, *110*, 2654–2665.
28. Reuel, N. F.; Dupont, A.; Thouvenin, O.; Lamb, D. C.; Strano, M. S. Three-Dimensional Tracking of Carbon Nanotubes within Living Cells. *ACS Nano* **2012**, *6*, 5420–5428.
29. Duque, J. G.; Cognet, L.; Parra-Vasquez, A. N. G.; Nicholas, N.; Schmidt, H. K.; Pasquali, M. Stable Luminescence from Individual Carbon Nanotubes in Acidic, Basic, and Biological Environments. *J. Am. Chem. Soc.* **2008**, *130*, 2626–2633.
30. Leeuw, T. K.; Reith, R. M.; Simonette, R. A.; Harden, M. E.; Cherukuri, P.; Tsyboulski, D. A.; Beckingham, K. M.; Weisman, R. B. Single-Walled Carbon Nanotubes in the Intact Organism: Near-IR Imaging and Biocompatibility Studies in *Drosophila*. *Nano Lett.* **2007**, *7*, 2650–2654.
31. Bose, S.; Khare, R. A.; Moldenaers, P. Assessing the Strengths and Weaknesses of Various Types of Pre-treatments of Carbon Nanotubes on the Properties of Polymer/Carbon Nanotubes Composites: A Critical Review. *Polymer* **2010**, *51*, 975–993.
32. Dyke, C. A.; Tour, J. M. Covalent Functionalization of Single-Walled Carbon Nanotubes for Materials Applications. *J. Phys. Chem. A* **2004**, *108*, 11151–11159.
33. Dyke, C. A.; Tour, J. M. Unbundled and Highly Functionalized Carbon Nanotubes from Aqueous Reactions. *Nano Lett.* **2003**, *3*, 1215–1218.
34. Ramesh, S.; Ericson, L. M.; Davis, V. A.; Saini, R. K.; Kittrell, C.; Pasquali, M.; Billups, W. E.; Adams, W. W.; Hauge, R. H.; Smalley, R. E. Dissolution of Pristine Single Walled Carbon Nanotubes in Superacids by Direct Protonation. *J. Phys. Chem. B* **2004**, *108*, 8794–8798.
35. Zhu, W.; Minami, N.; Kazaoui, S.; Kim, Y. π-Chromophore-Functionalized SWNTs by Covalent Bonding: Substantial Change in the Optical Spectra Proving Strong Electronic Interaction. *J. Mater. Chem.* **2004**, *14*, 1924.
36. Moore, V. C.; Strano, M. S.; Haroz, E. H.; Hauge, R. H.; Smalley, R. E.; Schmidt, J.; Talmon, Y. Individually Suspended Single-Walled Carbon Nanotubes in Various Surfactants. *Nano Lett.* **2003**, *3*, 1379–1382.
37. Arutyunyan, N. R.; Baklashev, D. V.; Obraztsova, E. D. Suspensions of Single-Wall Carbon Nanotubes Stabilized by Pluronic for Biomedical Applications. *Eur. Phys. J. B* **2010**, *75*, 163–166.
38. Nepal, D.; Geckeler, K. E. Proteins and Carbon Nanotubes: Close Encounter in Water. *Small* **2007**, *3*, 1259–1265.
39. Zheng, M.; Jagota, A.; Strano, M. S.; Santos, A. P.; Barone, P.; Chou, S. G.; Diner, B. A.; Dresselhaus, M. S.; McLean, R. S.; Onoa, G. B.; *et al.* Structure-Based Carbon Nanotube Sorting by Sequence-Dependent DNA Assembly. *Science* **2003**, *302*, 1545–1548.

40. Lucas, A.; Zakri, C.; Maugey, M.; Pasquali, M.; van der Schoot, P.; Poulin, P. Kinetics of Nanotube and Microfiber Scission under Sonication. *J. Phys. Chem. C* **2009**, *113*, 20599–20605.
41. Iamsamai, C.; Hannongbua, S.; Ruktanonchai, U.; Soottitantawat, A.; Dubas, S. T. The Effect of the Degree of Deacetylation of Chitosan on Its Dispersion of Carbon Nanotubes. *Carbon* **2010**, *48*, 25–30.
42. Yan, L. Y.; Poon, Y. F.; Chan-Park, M. B.; Chen, Y.; Zhang, Q. Individually Dispersing Single-Walled Carbon Nanotubes with Novel Neutral pH Water-Soluble Chitosan Derivatives. *J. Phys. Chem. C* **2008**, *112*, 7579–7587.
43. Yu, C.; Young, S.; Russo, V.; Amsden, B. G.; Flynn, L. E. Techniques for the Isolation of High Quality RNA from Cells Encapsulated in Chitosan Hydrogels. *Tissue Eng., Part C* **2013**, *19*, 829–838.
44. Madihally, S. V.; Matthew, H. W. Porous Chitosan Scaffolds for Tissue Engineering. *Biomaterials* **1999**, *20*, 1133–1142.
45. Pok, S.; Myers, J. D.; Madihally, S. V.; Jacot, J. G. A Multi-layered Scaffold of a Chitosan and Gelatin Hydrogel Supported by a PCL Core for Cardiac Tissue Engineering. *Acta Biomater.* **2013**, *9*, 5630–5642.
46. Pok, S. W.; Wallace, K. N.; Madihally, S. V. *In Vitro* Characterization of Polycaprolactone Matrices Generated in Aqueous Media. *Acta Biomater.* **2010**, *6*, 1061–1068.
47. Bachilo, S. M.; Strano, M. S.; Kittrell, C.; Hauge, R. H.; Smalley, R. E.; Weisman, R. B. Structure-Assigned Optical Spectra of Single-Walled Carbon Nanotubes. *Science* **2002**, *298*, 2361–2366.
48. O'Connell, M. J.; Bachilo, S. M.; Huffman, C. B.; Moore, V. C.; Strano, M. S.; Haroz, E. H.; Rialon, K. L.; Boul, P. J.; Noon, W. H.; Kittrell, C.; *et al.* Band Gap Fluorescence from Individual Single-Walled Carbon Nanotubes. *Science* **2002**, *297*, 593–596.
49. Liao, C. Z.; Li, K.; Wong, H. M.; Tong, W. Y.; Yeung, K. W. K.; Tjong, S. C. Novel Polypropylene Biocomposites Reinforced with Carbon Nanotubes and Hydroxyapatite Nanorods for Bone Replacements. *Mater. Sci. Eng., C* **2013**, *33*, 1380–1388.
50. Ferris, C. J.; In Het Panhuis, M. Conducting Bio-Materials Based on Gellan Gum Hydrogels. *Soft Matter* **2009**, *5*, 3430–3437.
51. Pok, S.; Jacot, J. G. Biomaterials Advances in Patches for Congenital Heart Defect Repair. *J. Cardiovasc. Transl. Res.* **2011**, *4*, 646–654.
52. Cirillo, G.; Hampel, S.; Spizzirri, U. G.; Parisi, O. I.; Picci, N.; Iemma, F. Carbon Nanotubes Hybrid Hydrogels in Drug Delivery: A Perspective Review. *BioMed. Res. Int.* **2014**, 17.
53. Satarkar, N. S.; Johnson, D.; Marrs, B.; Andrews, R.; Poh, C.; Gharaibeh, B.; Saito, K.; Anderson, K. W.; Hilt, J. Z. Hydrogel−MWCNT Nanocomposites: Synthesis, Characterization, and Heating with Radiofrequency Fields. *J. Appl. Polym. Sci.* **2010**, *117*, 1813–1819.
54. Tamaddon, M.; Walton, R. S.; Brand, D. D.; Czernuszka, J. T. Characterisation of Freeze-Dried Type II Collagen and Chondroitin Sulfate Scaffolds. *J. Mater. Sci.: Mater. Med.* **2013**, *24*, 1153–1165.
55. Grady, B. P. The Use of Solution Viscosity To Characterize Single-Walled Carbon Nanotube Dispersions. *Macromol. Chem. Phys.* **2006**, *207*, 2167–2169.
56. Kamata, H.; Akagi, Y.; Kayasuga-Kariya, Y.; Chung, U.-i.; Sakai, T. "Nonswellable" Hydrogel without Mechanical Hysteresis. *Science* **2014**, *343*, 873–875.
57. Bhattacharyya, S.; Guillott, S.; Dabboue, H.; Tranchant, J.-F.; Salvetat, J.-P. Carbon Nanotubes as Structural Nanofibers for Hyaluronic Acid Hydrogel Scaffolds. *Biomacromolecules* **2008**, *9*, 505–509.
58. Zanello, L. P.; Zhao, B.; Hu, H.; Haddon, R. C. Bone Cell Proliferation on Carbon Nanotubes. *Nano Lett.* **2006**, *6*, 562–567.
59. Mooney, E.; Dockery, P.; Greiser, U.; Murphy, M.; Barron, V. Carbon Nanotubes and Mesenchymal Stem Cells: Biocompatibility, Proliferation and Differentiation. *Nano Lett.* **2008**, *8*, 2137–2143.
60. Ghaly, H.; Boyle, P.; Vigmond, E.; Nygren, A. Reduced Conduction Reserve of the Propagating Cardiac Impulse in the Diabetic Rat Heart: A Model Study. *Conf. Proc. IEEE Eng. Med. Biol. Soc.* **2008**, 5926–5929.
61. Radisic, M.; Fast, V. G.; Sharifov, O. F.; Iyer, R. K.; Park, H.; Vunjak-Novakovic, G. Optical Mapping of Impulse Propagation in Engineered Cardiac Tissue. *Tissue Eng., Part A* **2009**, *15*, 851–860.
62. Sun, L. S.; Legato, M. J.; Rosen, T. S.; Steinberg, S. F.; Rosen, M. R. Sympathetic Innervation Modulates Ventricular Impulse Propagation and Repolarization in the Immature Rat-Heart. *Cardiovasc. Res.* **1993**, *27*, 459–463.
63. Rohr, S.; Schölly, D. M.; Kléber, A. G. Patterned Growth of Neonatal Rat Heart Cells in Culture. Morphological and Electrophysiological Characterization. *Circ. Res.* **1991**, *68*, 114–130.
64. Naumov, A. V.; Kuznetsov, O. A.; Harutyunyan, A. R.; Green, A. A.; Hersam, M. C.; Resasco, D. E.; Nikolaev, P. N.; Weisman, R. B. Quantifying the Semiconducting Fraction in Single-Walled Carbon Nanotube Samples through Comparative Atomic Force and Photoluminescence Microscopies. *Nano Lett.* **2009**, *9*, 3203–3208.
65. Carver, R. L.; Peng, H.; Sadana, A. K.; Nikolaev, P.; Arepalli, S.; Scott, C. D.; Billups, W. E.; Hauge, R. H.; Smalley, R. E. A Model for Nucleation and Growth of Single Wall Carbon Nanotubes *via* the HiPco Process: A Catalyst Concentration Study. *J. Nanosci. Nanotechnol.* **2005**, *5*, 1035–1040.
66. Chiang, I. W.; Brinson, B. E.; Huang, A. Y.; Willis, P. A.; Bronikowski, M. J.; Margrave, J. L.; Smalley, R. E.; Hauge, R. H. Purification and Characterization of Single-Wall Carbon Nanotubes (SWNTs) Obtained from the Gas-Phase Decomposition of CO (HiPco Process). *J. Phys. Chem. B* **2001**, *105*, 8297–8301.
67. Bronikowski, M. J.; Willis, P. A.; Colbert, D. T.; Smith, K. A.; Smalley, R. E. Gas-Phase Production of Carbon Single-Walled Nanotubes from Carbon Monoxide *via* the HiPco Process: A Parametric Study. *J. Vac. Sci. Technol., A* **2001**, *19*, 1800.
68. Kukovecz, A.; Kramberger, C.; Georgakilas, V.; Prato, M.; Kuzmany, H. A Detailed Raman Study on Thin Single-Wall Carbon Nanotubes Prepared by the HiPCO Process. *Eur. Phys. J. B* **2002**, *28*, 223–230.
69. Behabtu, N.; Young, C. C.; Tsentalovich, D. E.; Kleinerman, O.; Wang, X.; Ma, A. W. K.; Bengio, E. A.; ter Waarbeek, R. F.; de Jong, J. J.; Hoogerwerf, R. E.; *et al.* Strong, Light, Multifunctional Fibers of Carbon Nanotubes with Ultrahigh Conductivity. *Science* **2013**, *339*, 182–186.
70. Parra-Vasquez, A. N. G.; Stepanek, I.; Davis, V. A.; Moore, V. C.; Haroz, E. H.; Shaver, J.; Hauge, R. H.; Smalley, R. E.; Pasquali, M. Simple Length Determination of Single-Walled Carbon Nanotubes by Viscosity Measurements in Dilute Suspensions. *Macromolecules* **2007**, *40*, 4043–4047.
71. Pagani, G.; Green, M. J.; Poulin, P.; Pasquali, M. Competing Mechanisms and Scaling Laws for Carbon Nanotube Scission by Ultrasonication. *Proc. Natl. Acad. Sci. U.S.A.* **2012**, *109*, 11599–11604.
72. Parra-Vasquez, A. N. G.; Duque, J. G.; Green, M. J. Assessment of Length and Bundle Distribution of Dilute Single-Walled Carbon Nanotubes by Viscosity Measurements. *AIChE* **2014**, *60*, 1499–1508.
73. Yui, T.; Imada, K.; Okuyama, K.; Obata, Y.; Suzuki, K.; Ogawa, K. Molecular and Crystal Structure of the Anhydrous form of Chitosan. *Macromolecules* **1994**, *27*, 7601–7605.
74. Sweetman, L. J.; Moulton, S. E.; Wallace, G. G. Characterisation of Porous Freeze Dried Conducting Carbon Nanotube−Chitosan Scaffolds. *J. Mater. Chem.* **2008**, *18*, 5417–5422.
75. Parra-Vasquez, A. N. G.; Behabtu, N.; Green, M. J.; Pint, C. L. Spontaneous Dissolution of Ultralong Single- and Multi-walled Carbon Nanotubes. *ACS Nano* **2010**, *4*, 3969–3978.
76. Davis, V. A.; Parra-Vasquez, A. N. G.; Green, M. J. True Solutions of Single-Walled Carbon Nanotubes for Assembly into Macroscopic Materials. *Nat. Nanotechnol.* **2009**, *4*, 830–834.
77. Rai, P. K.; Pinnick, R. A.; Parra-Vasquez, A. N. G.; Davis, V. A.; Schmidt, H. K.; Hauge, R. H.; Smalley, R. E.; Pasquali, M. Isotropic-Nematic Phase Transition of Single-Walled Carbon Nanotubes in Strong Acids. *J. Am. Chem. Soc.* **2006**, *128*, 591–595.

78. Kumirska, J.; Czerwicka, M.; Kaczyński, Z.; Bychowska, A.; Brzozowski, K.; Thöming, J.; Stepnowski, P. Application of Spectroscopic Methods for Structural Analysis of Chitin and Chitosan. *Mar. Drugs* **2010**, *8*, 1567–1636.
79. Sakai, S.; Hirose, K.; Taguchi, K.; Ogushi, Y.; Kawakami, K. An Injectable, *In Situ* Enzymatically Gellable, Gelatin Derivative for Drug Delivery and Tissue Engineering. *Biomaterials* **2009**, *30*, 3371–3377.
80. Mi, F.-L. Synthesis and Characterization of a Novel Chitosan−Gelatin Bioconjugate with Fluorescence Emission. *Biomacromolecules* **2005**, *6*, 975–987.
81. Jacot, J. G.; McCulloch, A. D.; Omens, J. H. Substrate Stiffness Affects the Functional Maturation of Neonatal Rat Ventricular Myocytes. *Biophys. J.* **2008**, *95*, 3479–3487.
82. Sondergaard, C. S.; Mathews, G.; Wang, L.; Jeffreys, A.; Sahota, A.; Wood, M.; Ripplinger, C. M.; Si, M.-S. Contractile and Electrophysiologic Characterization of Optimized Self-Organizing Engineered Heart Tissue. *Ann. Thorac. Surg.* **2012**, *94*, 1241–1249.
83. Zong, X. H.; Bien, H.; Chung, C. Y.; Yin, L. H.; Fang, D. F.; Hsiao, B. S.; Chu, B.; Entcheva, E. Electrospun Fine-Textured Scaffolds for Heart Tissue Constructs. *Biomaterials* **2005**, *26*, 5330–5338.